QUANTUM INFORMATION PROCESSING AND PRECISE OPTICAL MEASUREMENT WITH HYPER-ENTANGLED QUANTUM STATES

A. V. Sergienko
Quantum Imaging Laboratory, Department of Electrical and Computer Engineering, Boston Univ. 8 Saint Mary's St., Boston MA 02215
Department of Physics, Boston Univ., 590 Commonwealth Ave., Boston MA 02215
alexserg@.edu

G. S. Jaeger
Quantum Imaging Laboratory, Department of Electrical and Computer Engineering, Boston Univ. 8 Saint Mary's St., Boston MA 02215
jaeger@bu.edu

G. Di Giuseppe
Quantum Imaging Laboratory, Department of Electrical and Computer Engineering, Boston Univ. 8 Saint Mary's St., Boston MA 02215
gdg@bu.edu

Bahaa E. A. Saleh
Quantum Imaging Laboratory, Department of Electrical and Computer Engineering, Boston Univ. 8 Saint Mary's St., Boston MA 02215
teich@bu.edu

Malvin C. Teich
Quantum Imaging Laboratory, Department of Electrical and Computer Engineering, Boston Univ. 8 Saint Mary's St., Boston MA 02215
Department of Physics, Boston Univ., 590 Commonwealth Ave., Boston MA 02215
teich@bu.edu

Abstract A pair of photons generated in the nonlinear process of spontaneous parametric down conversion is, in general, entangled so as to contain strong energy, time, polarization, and momentum quantum correlations. This entanglement involving more than one pair of quantum variable, known as hyper-entanglement, serves as a powerful tool in fundamental studies of foundations of the quantum theory, in the development of novel information processing techniques, and in the construction of new quantum measurement technologies, such as quantum ellipsometry.

Keywords: Quantum information/ quantum optics/ quantum communication/ entanglement/ quantum technology

1. Introduction

Entangled-photon states produced by spontaneous parametric down- conversion provide a natural basis for quantum measurement and quantum information processing, because they are not prone to decoherence and are composed of photons that remain higher correlated even after propagating to widely separated locations in space. The strong quantum correlations naturally present between down-conversion photons allow for uniquely quantum mechanical forms of measurement to be performed, which offer advantages over their classical counterparts. These states also allow quantum information to be encoded, and their robust coherence allows information to be processed in uniquely quantum mechanical ways. In order to realize the full potential of entangled-photon states, it is vital to understand and exploit all those features present in their quantum states from the point of their creation, during their propagation and until their detection. Here we consider such states of multi-photons produced by spontaneous parametric down-conversion (SPDC). The unique properties of quantum systems captured by these states are strikingly manifested when quantum intensity correlation interferometry is performed.

Quantum-interference patterns generally arise in contexts where only a single parameter, such as polarization, is actively manipulated. However, it has been shown [1] that by making use of all the parameters naturally relevant one can, in fact, modify the interference pattern associated with one parameter such as polarization, by manipulating others, such as the frequency and transverse wave vector. This interdependence of physical parameters has its origin in the non-factorizability of the quantum state produced in the process of spontaneous parametric down-conversion (SPDC) into a product of functions of single parameters, such as polarization, frequency and wave-vector. For example, inconsistencies between existing theoretical models and the results of femtosecond down-conversion experiments commonly arise as a result of failing to consider the full Hilbert space occupied by the entangled quantum state, with its dependency on multiple variables. In particular, femtosecond SPDC models have ignored transverse wave-vector components and, as a result, have not accounted for the previously demonstrated angular spread of such down-

converted light [2]. However, a comprehensive approach to quantum states, such as has been recently pursued, permits intelligent engineering of quantum states. This approach will be discussed in the following section.

In many practical applications, technology can benefit from the fact that, though each individual subsystem may actually possess inherent uncertainties, the components of the entangled pair may exhibit no such uncertainty relative to one another. One can exploit this unique aspect of entanglement for the development of a new class of optical measurements, those of quantum optical metrology. Entangled states have been used with great effectiveness during the last twenty years for carrying out striking experiments, for example those demonstrating non-local dispersion cancellation [3], entangled-photon-induced transparency [4], and entangled-photon spectroscopy with monochromatic light [5]. The practical availability of entangled beams has made it possible to conduct such fundamental physics experiments without having to resort to costly instruments such as particle colliders and synchrotrons. A new generation of techniques for quantum metrology and quantum information processing is under development, which will be discussed in detail in following sections.

Entangled photons first became of interest in probing the foundations of quantum theory. The often deeply counterintuitive predictions of quantum mechanics have been the focus of intensive discussions and debates among physicists since the introduction of the formal theory in the 1930's. Since then, entangled states of increasing quality have been prepared in order to progressively better differentiate quantum behavior from classical behavior. Entangled quantum systems are composed of at least two component subsystems and are described by states that cannot be written as a product of independent subsystem states,

$$|\Psi\rangle \neq |\psi_1\rangle \otimes |\psi_2\rangle \ , \tag{1}$$

for *any* two quantum states $|\psi_n\rangle$ of the individual subsystems. Schrödinger [6], who first defined entanglement, stated, called entanglement "the characteristic trait of quantum mechanics." In 1935, Einstein, Podolsky and Rosen (EPR) [7] presented an influential argument based on analyzing entangled states of two systems described by infinite superpositions of such as

$$|\Psi(x_1, x_2)\rangle = \sum_{i=1}^{\infty} c_n(x_1, x_2)|\psi_n(x_1)\rangle|\phi_n(x_2)\rangle \ , \tag{2}$$

where the ψ_i and ϕ_i are elements of orthogonal state bases, that quantum mechanics is an incomplete theory of physical objects, as judged from the perspective of metaphysical realism.

This theoretical argument was later followed by experiments by Wu and Shaknov [8] on electron-positron singlets that amounted to practical tests of

nonclassical behavior. Simpler entangled states such as these,

$$|\Psi\rangle = \frac{1}{\sqrt{2}}(|\uparrow\rangle|\downarrow\rangle - |\downarrow\rangle|\uparrow\rangle) \,, \tag{3}$$

were discussed by David Bohm [9] and analyzed by Bohm and Aharonov [10]. The systematic study of quantum-scale behavior that could not be explained by the class of local, deterministic hidden variables theories then began, with a focus on such states of strongly entangled particle pairs. In 1964, John Bell derived a general inequality that introduced a clear empirical boundary between local, classically explicable behavior and less intuitive forms of behavior, involving a notion that he called "nonlocality" [11].

By the early 1980s, advances in laser physics and optics had allowed for an entirely new generation of experiments by the group of Aspect at Orsay, France based on the use of photon pairs produced by nonlinear laser excitations of an atomic radiative cascade [12]. These experiments paved the way for future quantum-interferometric experiments involving entangled photons, finally producing an unambiguous violation of a Bell-type inequality by tens of standard deviations and strong agreement with quantum-mechanical predictions. By that time, a more powerful source of entangled photons, the optical parametric oscillator (OPO), had also already been developed, independently of tests of basic principles of quantum mechanics. Indeed, OPOs were operational in major nonlinear optics research groups around the world almost immediately following the development of the laser (for more details, see [13]). Shortly after the first OPOs were introduced, a number of experimental groups independently discovered the spontaneous emission of polarized photons in an optical parametric amplifier. OPO spontaneous noise, which was very weak, occupied a very broad spectral range, from near the blue pump frequency through to the infrared absorption band. A corresponding spatial distribution of different frequencies followed the well known and simple phase-matching conditions of nonlinear optical systems.

The statistics of photons appearing in such spontaneous conversion of one photon into a pair had been analyzed in the 1960s, demonstrating the very strong correlations between these photons in space, time and frequency. Burnham and Weinberg [14] first demonstrated the unique and explicitly nonclassical features of states of two-photons generated in the spontaneous regime from the parametric amplifier. Quantum correlations involving photon pairs were exploited again 10 years later in experimental work by Malygin, Penin and Sergienko [15]. The use of highly correlated pairs of photons for the explicit demonstration of Bell inequality violations has become popular and convenient since the mid-1980s and has been widely exploited since then. The process of generating these states is now known as "spontaneous parametric down-conversion"

(SPDC), and has become widely utilized. New, high-intensity sources of SPDC have been developed over the last two decades (see, for example, [16]).

Spontaneous parametric down-conversion of one photon into a pair is said to be of one of two types, based on the satisfaction of "phase-matching" conditions of either type I or of type II, corresponding to whether the two photons of the down-conversion pair have the same polarization or orthogonal polarizations, respectively. The two photons of a pair can also leave the down-converting medium either in the same direction or in different directions, referred to as the collinear and non-collinear cases, respectively. A medium is required for down-conversion, as conservation laws exclude the decay of one photon into a pair in vacuum. The medium is usually some sort of birefringent crystal, such as potassium dihydrogen phosphate (KDP), having a $\chi^{(2)}$ optical nonlinearity. Upon striking such a nonlinear crystal, there is a small probability (on the order of 10^{-7}) that an incident pump photon will be down-converted into a two-photon (see Fig. 1). If down-conversion occurs, these conserved quantities

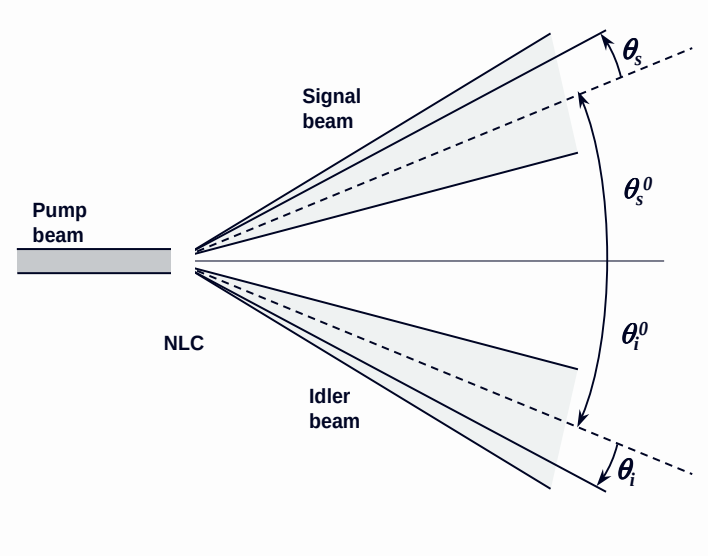

Figure 1. Spontaneous parametric down-conversion [17].

are carried into that of the resulting photon pair under the constraints of their respective conservation laws, so that the phases of the corresponding wave-functions match, in accordance with the relations

$$\omega_s + \omega_i = \omega_p, \quad k_s + k_i = k_p, \tag{4}$$

referred to as the phase-matching conditions, where the k_i and ω_i are momenta and frequencies for the three waves involved. The individual photons resulting from down-conversion are often arbitrarily called "signal" (s) and "idler" (i), for historical reasons.

When the two photons of a pair have different momenta or energies, entanglement will arise in SPDC, provided that the alternatives are in principle experimentally indistinguishable. The two-photon state produced in type-I down-conversion can be written

$$|\Psi\rangle = \sum_{s,i} \delta(\omega_s + \omega_i - \omega_p)\delta(k_s + k_i - k_p)|k_s\rangle \otimes |k_i\rangle \ . \tag{5}$$

In this case, the two photons leave the nonlinear medium with the same polarization, namely that orthogonal to the polarization of the pump beam. Down-conversion photons are thus produced in two thick spectral cones, one for each photon, within which two-photons appear each as a pair of photons on opposite sides of the pump-beam direction (see Fig. 1). In the mid-1980s, Hong, Ou and

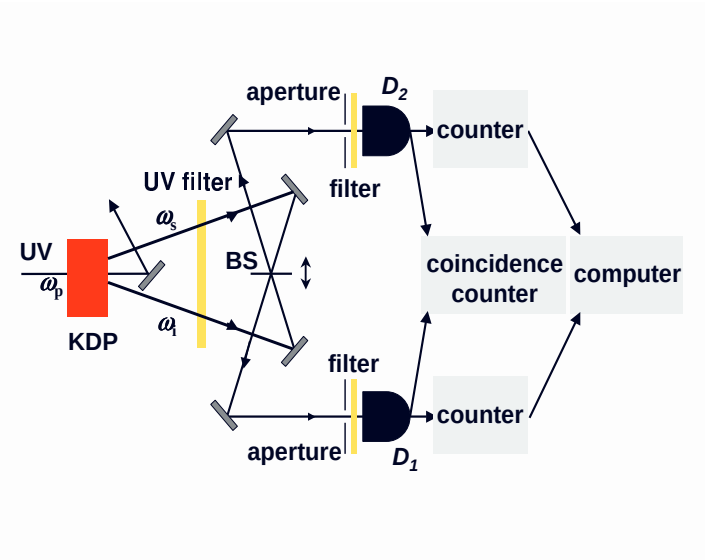

Figure 2. Hong-Ou-Mandel interferometer [18].

Mandel [18] created noncollinear, type-I phase-matched SPDC photon pairs in KDP crystal using an ultraviolet continuous-wave (cw) laser pump beam (see Fig. 2). This experiment empirically demonstrated the strong temporal correlation of the two-photons. Filters were placed in the apparatus, determining the frequency spread of the down-converted photons permitted to interfere. Since

this experiment, the common approach to quantum interferometry has been to choose a single entangled parameter of interest and to eliminate the dependence of the quantum state on all other parameters. For example, when investigating polarization entanglement, strong spectral and spatial filtering are typically imposed in an attempt to restrict attention to the polarization variable alone.

A more general approach to this problem is to exploit the multi-faceted nature of photon entanglement from the outset. In such an approach, the observed quantum-interference pattern in one parameter, such as polarization, can be modified by controlling the dependence of the state on the other parameters, such as frequency and transverse wave vector. A more complete theory of spontaneous parametric down-conversion allows us to understand the full character of fourth-order quantum interference in many valuable experiments. SPDC gives rise to a quantum state that is entangled in multiple parameters, such as three-dimensional wave-vector and polarization. Many experiments designed to verify the non-factorizability of classes of quantum states, the mathematical essence of entanglement, are carried out in the context of models that fail to consider the overall relevant Hilbert space and are restricted to entanglement of only a single aspect of the quantum state, such as energy [19], momentum [20], or polarization [21]. Indeed, inconsistencies emerge in the analysis of quantum-interferometric experiments involving down-conversion under such circumstances, a fact that has been highlighted by the failure of the conventional theory of ultrafast parametric down-conversion to characterize quantum-interference experiments. This is because femtosecond SPDC models have ignored transverse wave-vector components and have thereby not accounted for the previously demonstrated angular spread of such down-converted light [22].

2. Hyperentangled State Engineering

In order to better understand the quantum systems produced in spontaneous parametric down-conversion and the possibilities they provide, it is useful to analyze their behavior during each of the three distinct stages of their passage through any experimental apparatus, that is, the generation, propagation, and detection of the two-photon optical state. Begining with quantum state generation, one can see how to take advantage of the state by systematically controlling it during propagation and to extract useful information through the use of of a properly chosen detection scheme [23].

2.1 Generation

The relatively weak interaction between the three modes of the electromagnetic field participating in SPDC within the nonlinear crystal allows us

to consider the two-photon state generated within the confines of first-order time-dependent perturbation theory. The two-photon state can be written

$$|\Psi^{(2)}\rangle \;\sim\; \frac{\mathrm{i}}{\hbar}\int_{t_0}^{t} dt'\; \hat{H}_{\mathrm{int}}(t')\;|0\rangle\,, \tag{6}$$

with the interaction Hamiltonian

$$\hat{H}_{int}(t) \sim \chi^{(2)}\int_V d\mathbf{r}\; \hat{E}_p^{(+)}(\mathbf{r},t)\hat{E}_o^{(-)}(\mathbf{r},t)\hat{E}_e^{(-)}(\mathbf{r},t) + H.c.\,, \tag{7}$$

where $\chi^{(2)}$ is the second-order susceptibility and V is the volume in which the interaction can take place. The field operator $\hat{E}_j^{(\pm)}(\mathbf{r},t)$ represents the positive-(negative-) frequency portion of the electric-field operator E_j, with the subscript j representing the pump (p), ordinary (o), and extraordinary (e) waves at position $\mathbf{r}$ and time t, and H.c. stands for Hermitian conjugate. The high intensity of the pump field allows one to represent it by a classical c-number, with an arbitrary spatiotemporal profile given by

$$E_p(\mathbf{r},t) = \int d\mathbf{k}_p\; \tilde{E}_p(\mathbf{k}_p)e^{i\mathbf{k}_p\cdot\mathbf{r}}e^{-\mathrm{i}\omega_p(\mathbf{k}_p)t}\,, \tag{8}$$

where $\tilde{E}_p(\mathbf{k}_p)$ is the complex-amplitude of the field, as a function of the wave-vector $\mathbf{k}_p$. Decomposing the three-dimensional wavevector $\mathbf{k}_p$ into two-dimensional transverse wavevector $\mathbf{q}_p$ and a frequency part ω_p, this is

$$E_p(\mathbf{r},t) = \int d\mathbf{q}_p\, d\omega_p\; \tilde{E}_p(\mathbf{q}_p;\omega_p)e^{\mathrm{i}\kappa_p z}e^{\mathrm{i}\mathbf{q}_p\cdot\mathbf{x}}e^{-\mathrm{i}\omega_p t}\,, \tag{9}$$

where $\mathbf{x}$ spans the transverse plane perpendicular to the propagation direction z, as illustrated in Fig. 3. The ordinary and extraordinary modes of the field can similarly be expressed in terms of the creation operators $\hat{a}^\dagger(\mathbf{q},\omega)$ as

$$\hat{E}_j^{(-)}(\mathbf{r},t) = \int d\mathbf{q}_j\, d\omega_j\; e^{-\mathrm{i}\kappa_j z}e^{-\mathrm{i}\mathbf{q}_j\cdot\mathbf{x}}e^{\mathrm{i}\omega_j t}\;\hat{a}_j^\dagger(\mathbf{q}_j,\omega_j)\,, \tag{10}$$

where $j = o, e$. The longitudinal component of momentum, $\mathbf{k}$, which we denote by κ, can be written in terms of the $(\mathbf{q},\omega)$ pair [24] as $\kappa = \sqrt{[n(\omega,\theta)\,\omega/c]^2 - |\mathbf{q}|^2}$, where c is the speed of light in vacuum, θ is the angle between $\mathbf{k}$ and the optical axis of the nonlinear crystal (see Fig. 3), and $n(\omega,\theta)$ is the index of refraction in the nonlinear medium.

The quantum state after the nonlinear crystal is thus

$$|\Psi^{(2)}\rangle \sim \int d\mathbf{q}_o d\mathbf{q}_e\, d\omega_o d\omega_e\; \Phi(\mathbf{q}_o,\mathbf{q}_e;\omega_o,\omega_e)\hat{a}_o^\dagger(\mathbf{q}_o,\omega_o)\hat{a}_e^\dagger(\mathbf{q}_e,\omega_e)|0\rangle\,, \tag{11}$$

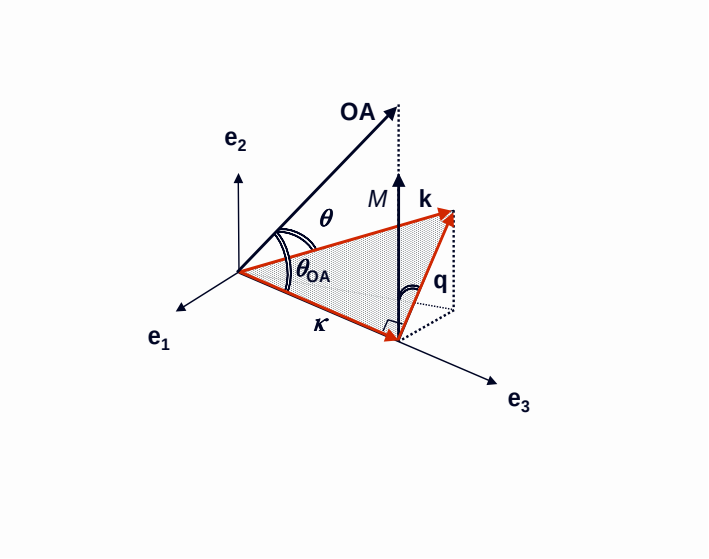

Figure 3. Decomposition of a three-dimensional wavevector (**k**) into longitudinal (κ) and transverse (**q**) components [23]. The angle between the optical axis of the nonlinear crystal (OA) and the wavevector **k** is θ. $\theta_{\rm OA}$ is the angle between the optical axis and the longitudinal axis ($\mathbf{e}_3$). The spatial walk-off of the extraordinary polarization component of a field travelling through the nonlinear crystal is characterized by M.

with

$$\Phi(\mathbf{q}_o,\mathbf{q}_e;\omega_o,\omega_e) \;=\; \tilde{E}_p(\mathbf{q}_o+\mathbf{q}_e;\omega_o+\omega_e)\,L\,\mathrm{sinc}\left(\frac{L\Delta}{2}\right)e^{-\mathrm{i}\frac{L\Delta}{2}}\,, \qquad (12)$$

where L is the thickness of the crystal and $\Delta=\kappa_p-\kappa_o-\kappa_e$, κ_j $(j=p,o,e)$ being related to the indices $(\mathbf{q}_j,\omega_j)$. Recall that the inextricable dependencies of the function $\Phi(\mathbf{q}_o,\mathbf{q}_e;\omega_o,\omega_e)$ on its several variables in Eqs. (11) and (12) is the essence of multi-parameter entanglement.

2.2 Propagation

Propagation of the down-converted light between the planes of generation and detection is described by the transfer function of the optical system. The photon-pair probability amplitude at the space-time points $(\mathbf{x}_A,t_A)$ and $(\mathbf{x}_B,t_B)$ of detection is defined by

$$A(\mathbf{x}_A,\mathbf{x}_B;t_A,t_B)=\langle 0|\hat{E}_A^{(+)}(\mathbf{x}_A,t_A)\hat{E}_B^{(+)}(\mathbf{x}_B,t_B)|\Psi^{(2)}\rangle\,, \qquad (13)$$

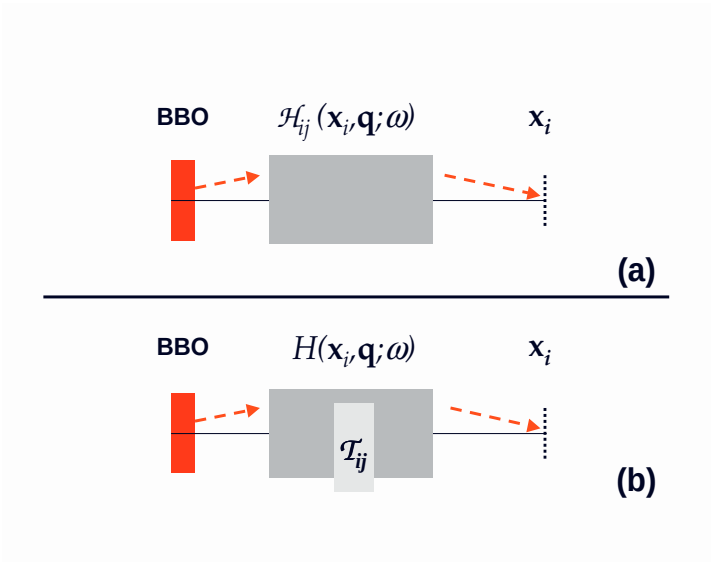

Figure 4. (a) Illustration of the idealized setup for observation of quantum interference using SPDC [23]. BBO represents a beta-barium borate nonlinear optical crystal, $\mathcal{H}_{ij}(\mathbf{x}_i,\mathbf{q};\omega)$ is the transfer function of the system, and the detection plane is represented by $\mathbf{x}_i$. (b) For most experimental configurations the transfer function can be factorized into diffraction-dependent $[H(\mathbf{x}_i,\mathbf{q};\omega)]$ and diffraction-independent ($\mathcal{T}_{ij}$) components.

where the quantum operators at the detection locations are [25]

$$\begin{aligned}\hat{E}_A^{(+)}(\mathbf{x}_A,t_A) = \int d\mathbf{q}\, d\omega\; e^{-\mathrm{i}\omega t_A}\,[\mathcal{H}_{Ae}(\mathbf{x}_A,\mathbf{q};\omega)\hat{a}_e(\mathbf{q},\omega)+\\ +\,\mathcal{H}_{Ao}(\mathbf{x}_A,\mathbf{q};\omega)\hat{a}_o(\mathbf{q},\omega)]\;,\\ \hat{E}_B^{(+)}(\mathbf{x}_B,t_B) = \int d\mathbf{q}\, d\omega\; e^{-\mathrm{i}\omega t_B}\,[\mathcal{H}_{Be}(\mathbf{x}_B,\mathbf{q};\omega)\hat{a}_e(\mathbf{q},\omega)+\\ +\mathcal{H}_{Bo}(\mathbf{x}_B,\mathbf{q};\omega)\hat{a}_o(\mathbf{q},\omega)]\;. \end{aligned} \tag{14}$$

The transfer function $\mathcal{H}_{ij}$ ($i = A, B$ and $j = e, o$) describes the propagation of a $(\mathbf{q},\omega)$ mode from the nonlinear-crystal output plane to the detection plane. The photon-pair probability amplitude is thus:

$$\begin{aligned}A(\mathbf{x}_A,\mathbf{x}_B;t_A,t_B) = \int d\mathbf{q}_o d\mathbf{q}_e\, d\omega_o d\omega_e \Phi(\mathbf{q}_o,\mathbf{q}_e;\omega_o,\omega_e)\\ \times\Big[\mathcal{H}_{Ae}(\mathbf{x}_A,\mathbf{q}_e;\omega_e)\mathcal{H}_{Bo}(\mathbf{x}_B,\mathbf{q}_o;\omega_o)\,e^{-\mathrm{i}(\omega_e t_A+\omega_o t_B)}\\ +\,\mathcal{H}_{Ao}(\mathbf{x}_A,\mathbf{q}_o;\omega_o)\mathcal{H}_{Be}(\mathbf{x}_B,\mathbf{q}_e;\omega_e)\,e^{-\mathrm{i}(\omega_o t_A+\omega_e t_B)}\Big]\;. \end{aligned} \tag{15}$$

By appropriately choosing the optical system, the overall probability amplitude can be constructed as desired. The influence of the optical system on the photon-pair wave-function appearts in the above expressions through the functions $\mathcal{H}_{Ae}$, $\mathcal{H}_{Ao}$, $\mathcal{H}_{Be}$, and $\mathcal{H}_{Bo}$.

2.3 Detection

The character of the detection process will depend on the nature of the apparatus. Slow detectors, for example, perform temporal integration while detectors of finite area perform spatial integration. One limit is that when the temporal response of a point detector is spread negligibly with respect to the characteristic time scale of SPDC, which is given by the inverse of down-conversion bandwidth. In this limit, the coincidence rate reduces to

$$R = |A(\mathbf{x}_A, \mathbf{x}_B; t_A, t_B)|^2 . \tag{16}$$

The other limit, typical of quantum-interference experiments, is reached as a result of the use of slow bucket detectors. In such a situation, the coincidence count rate R is given in terms of the photon-pair probability amplitude by

$$R = \int d\mathbf{x}_A d\mathbf{x}_B \, dt_A dt_B \, |A(\mathbf{x}_A, \mathbf{x}_B; t_A, t_B)|^2 . \tag{17}$$

2.4 Engineering Basics

Having completed this formal analysis, one can begin to consider specific configurations of a quantum interferometer that might take practical advantage of the multiple parameter dependence of hyperentangled quantum states. This choice corresponds to a specific form of the the transfer function $\mathcal{H}_{ij}$. Almost all quantum-interference experiments performed to date have the common feature that $\mathcal{H}_{ij}$ in Eq. (14), with $i = A, B$ and $j = o, e$, can be separated into diffraction-dependent and polarization-dependent terms as

$$\mathcal{H}_{ij}(\mathbf{x}_i, \mathbf{q}; \omega) \; = \; \mathcal{T}_{ij} \, H(\mathbf{x}_i, \mathbf{q}; \omega), \tag{18}$$

where the diffraction-dependent terms are grouped in H and the diffraction-independent terms are grouped in $\mathcal{T}_{ij}$ (see Fig. 4). Free space, apertures, and lenses, for example, can be treated as diffraction-dependent elements while beam splitters and waveplates can be considered as diffraction-independent elements.

For example, in collinear SPDC configurations in the presence of a relative optical-path delay τ between the ordinary and the extraordinary polarized photons, $\mathcal{T}_{ij}$ is $\mathcal{T}_{ij} = (\mathbf{e}_i \cdot \mathbf{e}_j) \, e^{-\mathrm{i}\omega\tau\delta_{ej}}$, where the δ_{ej} is the Kronecker delta, with $\delta_{ee} = 1$ and $\delta_{eo} = 0$, the unit vector $\mathbf{e}_i$ specifies the orientation of each

polarization analyzer in the experimental apparatus, and $\mathbf{e}_j$ is the unit vector that describes the polarization of each down-converted photon.

The general photon-pair probability amplitude given in Eq. (14), can be separated into diffraction-dependent and -independent elements:

$$\begin{aligned} A(\mathbf{x}_A,\mathbf{x}_B;t_A,t_B) = \int d\mathbf{q}_o d\mathbf{q}_e\, d\omega_o d\omega_e\; \Phi(\mathbf{q}_o,\mathbf{q}_e;\omega_o,\omega_e) \\ \times \Big[\mathcal{T}_{Ae} H(\mathbf{x}_A,\mathbf{q}_e;\omega_e)\mathcal{T}_{Bo} H(\mathbf{x}_B,\mathbf{q}_o;\omega_o)\, e^{-\mathrm{i}(\omega_e t_A+\omega_o t_B)} \\ +\mathcal{T}_{Ao} H(\mathbf{x}_A,\mathbf{q}_o;\omega_o)\mathcal{T}_{Be} H(\mathbf{x}_B,\mathbf{q}_e;\omega_e)\, e^{-\mathrm{i}(\omega_o t_A+\omega_e t_B)}\Big]. \end{aligned} \tag{19}$$

Taking the angle between $\mathbf{e}_i$ and $\mathbf{e}_j$ to be 45°, $\mathcal{T}_{ij}$ can be simplified by using $(\mathbf{e}_i\cdot\mathbf{e}_j)=\pm\frac{1}{\sqrt{2}}$ [21], and the photon-pair probability amplitude can be written

$$\begin{aligned} A(\mathbf{x}_A,\mathbf{x}_B;t_A,t_B) = \int d\mathbf{q}_o d\mathbf{q}_e\, d\omega_o d\omega_e\; \tilde{E}_p(\mathbf{q}_o+\mathbf{q}_e;\omega_o+\omega_e)\, L \\ \times \mathrm{sinc}\left(\frac{L\Delta}{2}\right) e^{-\mathrm{i}\frac{L\Delta}{2}}\, e^{-\mathrm{i}\omega_e\tau} \\ \times \Big[\, H(\mathbf{x}_A,\mathbf{q}_e;\omega_e) H(\mathbf{x}_B,\mathbf{q}_o;\omega_o)\, e^{-\mathrm{i}(\omega_e t_A+\omega_o t_B)} \\ -H(\mathbf{x}_A,\mathbf{q}_o;\omega_o) H(\mathbf{x}_B,\mathbf{q}_e;\omega_e)\, e^{-\mathrm{i}(\omega_o t_A+\omega_e t_B)}\Big]. \end{aligned} \tag{20}$$

Substitution of Eq. (19) into Eq. (17) provides the coincidence-count rate, given an arbitrary pump profile and optical system.

The diffraction-dependent elements in most of these experimental arrangements are illustrated in Fig. 5(b). To describe this system via the function H, one needs to derive the impulse response function (the point-spread function) for these optical systems. A typical aperture diameter of $b=1$ cm at a distance $d=1$ m from the crystal output plane yields $b^4/4\lambda d^3 < 10^{-2}$ using $\lambda = 0.5$ μm, guaranteeing the validity of the Fresnel approximation. Without loss of generality, one can use a two-dimensional (one longitudinal, one transverse dimension) analysis of the impulse response function. The extension to three dimensions is then straightforward. The impulse response function of the full optical system, from the crystal output plane to the detector input plane is

$$\begin{aligned} h(x_i,x;\omega) = \mathcal{F}(\omega)\, e^{\mathrm{i}\frac{\omega}{c}(d_1+d_2+f)}\, e^{-\mathrm{i}\frac{\omega x_i^2}{2cf}\left[\frac{d_2}{f}-1\right]} e^{\mathrm{i}\frac{\omega x^2}{2cd_1}} \\ \int dx' p(x') e^{\mathrm{i}\frac{\omega x'^2}{2cd_1}}\, e^{-\mathrm{i}\frac{\omega}{c}x'\left[\frac{x}{d_1}+\frac{x_i}{f}\right]}, \end{aligned} \tag{21}$$

which allows one to determine the transfer function of the system to be determined in terms of transverse wave-vectors via

$$H(\mathbf{x}_i,\mathbf{q};\omega) = \int d\mathbf{x}\, h(\mathbf{x}_i,\mathbf{x};\omega)\, e^{\mathrm{i}\mathbf{q}\cdot\mathbf{x}}, \tag{22}$$

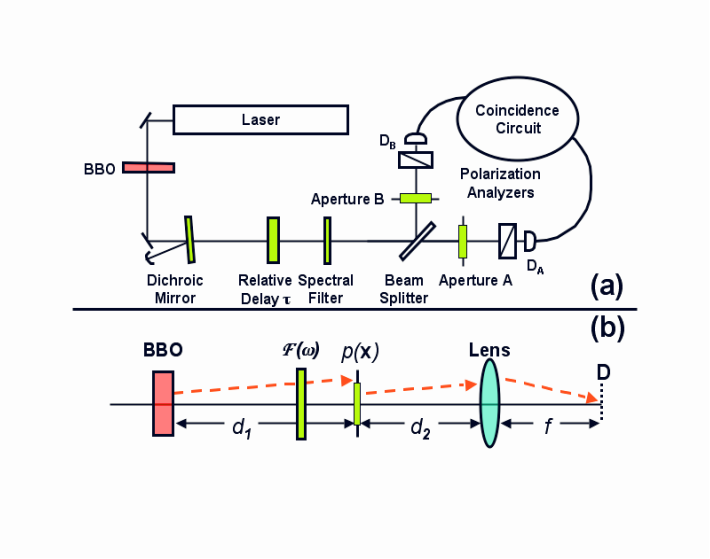

Figure 5. (a) Schematic of the experimental setup for observation of quantum interference using type-II collinear SPDC [23]. (b) The path from the crystal output plane to the detector input plane. $\mathcal{F}(\omega)$ represents an (optional) filter transmission function, $p(\mathbf{x})$ is an aperture function, and f is the focal length of the lens.

so that the transfer function takes the explicit form

$$H(\mathbf{x}_i,\mathbf{q};\omega)=\left[e^{\mathrm{i}\frac{\omega}{c}(d_1+d_2+f)}e^{-\mathrm{i}\frac{\omega|\mathbf{x}_i|^2}{2cf}\left[\frac{d_2}{f}-1\right]}e^{-\mathrm{i}\frac{cd_1}{2\omega}|\mathbf{q}|^2}\tilde{P}\left(\frac{\omega}{cf}\mathbf{x}_i-\mathbf{q}\right)\right]\mathcal{F}(\omega), \tag{23}$$

where $\tilde{P}\left(\frac{\omega}{cf}\mathbf{x}_i-\mathbf{q}\right)$ is

$$\tilde{P}\left(\frac{\omega}{cf}\mathbf{x}_i-\mathbf{q}\right)=\int d\mathbf{x}'p(\mathbf{x}')e^{-\mathrm{i}\frac{\omega\mathbf{x}'\cdot\mathbf{x}_i}{cf}}e^{\mathrm{i}\mathbf{q}\cdot\mathbf{x}'}\,. \tag{24}$$

Using Eq. (23) one can now describe the propagation of the down-converted light from the crystal to the detection planes. Note that, since no birefringence is assumed, this transfer function is the same for both polarization modes (*o*,*e*).

Continuing the analysis in the Fresnel approximation and using the approximation that the SPDC fields are quasi-monochromatic, one finds the form of the coincidence-count rate defined in Eq. (17):

$$R(\tau)=R_0\left[1-V\left(\tau\right)\right]\,, \tag{25}$$

where R_0 is the coincidence rate outside the region of quantum interference. In the absence of spectral filtering, we have

$$V(\tau) = \Lambda\left(\frac{2\tau}{LD} - 1\right)\ \mathrm{sinc}\left[\frac{\omega_p^0 L^2 M^2}{4cd_1}\frac{\tau}{LD}\,\Lambda\left(\frac{2\tau}{LD} - 1\right)\right] \tilde{\mathcal{P}}_A\left(-\frac{\omega_p^0 LM}{4cd_1}\frac{2\tau}{LD}\mathbf{e}_2\right)\,\tilde{\mathcal{P}}_B\left(\frac{\omega_p^0 LM}{4cd_1}\frac{2\tau}{LD}\mathbf{e}_2\right), \tag{26}$$

where $D = 1/u_o - 1/u_e$ with u_j denoting the group velocity for the j-polarized photon ($j = o, e$), $M = \partial \ln n_e(\omega_p^0/2, \theta_{\mathrm{OA}})/\partial\theta_e$, $\Lambda(x) = 1 - |x|$ for $-1 \leq x \leq 1$ and zero otherwise, and $\tilde{\mathcal{P}}_i$ (with $i = A, B$) is the normalized Fourier transform of the squared magnitude of the aperture function $p_i(\mathbf{x})$:

$$\tilde{\mathcal{P}}_i(\mathbf{q}) = \frac{\int\int d\mathbf{y}\; p_i(\mathbf{y}) p_i^*(\mathbf{y})\; e^{-\mathrm{i}\mathbf{y}\cdot\mathbf{q}}}{\int\int d\mathbf{y}\; p_i(\mathbf{y}) p_i^*(\mathbf{y})}\,. \tag{27}$$

The profile of the function $\tilde{\mathcal{P}}_i$ within Eq. (25) plays a key role in our analysis.

Extremely small apertures are commonly used to reach the one-dimensional plane wave limit. However, the interest here is in just those effects that this excludes. As shown in Eq. (25), this gives $\tilde{\mathcal{P}}_i$ functions that are broad in comparison with Λ, so that Λ determines the shape of the quantum interference pattern, resulting in a symmetric triangular dip. The sinc function in Eq. (25) is approximately equal to unity for all practical experimental configurations, and therefore plays an insignificant role. On the other hand, this sinc function represents the difference between the familiar one-dimensional model (which predicts $R(\tau) = R_0\left[1 - \Lambda\left(\frac{2\tau}{LD} - 1\right)\right]$, a perfectly triangular interference dip) and a three-dimensional model in the presence of a very small on-axis aperture. It is clear from Eq. (25) that $V(\tau)$ can be altered dramatically by carefully selecting the aperture profile.

2.5 Realizations

These results allow one to go about quantum state engineering in a systematic fashion in various situations. For example, consider the effect on quantum interference of polarization of a circular aperture of diameter b. Both the aperture shape and size, via the function $\tilde{P}(\mathbf{q})$, will have significant effects on the polarization quantum-interference patterns. Such an aperture can be described by the Bessel function J_1,

$$\tilde{\mathcal{P}}(\mathbf{q}) = 2\,\frac{J_1\left(b\,|\mathbf{q}|\right)}{b\,|\mathbf{q}|}\,. \tag{28}$$

Consider the experimental arrangement illustrated in Fig. 5(a). An experiment has been performed with SPDC with the pump being a single-mode cw

argon-ion laser with a wavelength of 351.1 nm and a power of 200 mW delivered to a β-$\mathrm{BaB_2O_4}$ (BBO) crystal with a thickness of 1.5 mm, aligned to produce collinear and degenerate Type-II spontaneous parametric down-conversion. Collinear down-conversion beams were sent through a delay line comprised of a z-cut crystalline quartz element (with its fast axis orthogonal to that of the BBO crystal) whose thickness was varied to control the relative optical-path delay between the photons of a down-converted pair. The characteristic thickness of the quartz element was much less than the distance between the crystal and the detection planes, yielding negligible effects on the spatial properties of the SPDC. The photon pairs were then sent to a non-polarizing beam splitter. Each arm of the polarization intensity interferometer following this beam splitter contained a Glan-Thompson polarization analyzer set to 45°, a convex lens to focus the incoming beam, and an actively quenched Peltier-cooled single-photon-counting avalanche photodiode detector [denoted D_A and D_B in Fig. 5(a)]. Note also that no spectral filtering was used in the selection of the signal and idler photons for detection. The counts from the detectors were conveyed to a coincidence counting circuit with a 3-ns coincidence-time window.

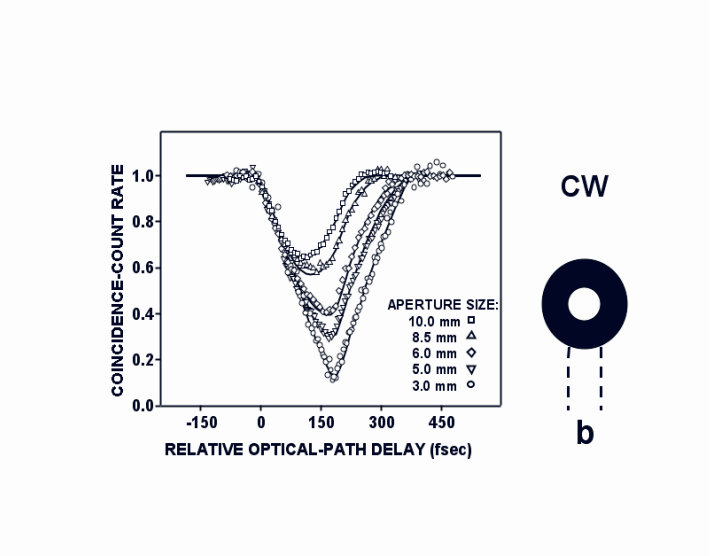

Figure 6. Normalized coincidence-count rate $R(\tau)/R_0$, as a function of the relative optical-path delay τ, for different diameters of a circular aperture placed 1 m from the crystal [23]. The symbols represent experimental results and the solid curves are theoretical plots. The dashed curve represents the one-dimensional (1D) plane wave theory, which is seen clearly to be inadequate for large aperture diameters.

For this situation involving a cw laser pump, the observed normalized coincidence rates correspond to the sort of quantum-interference pattern displayed in Fig. 6, as relative optical-path delay is varied, for various values of aperture diameter b placed 1 m from the crystal. The observed interference pattern is seen to be more strongly asymmetric for larger values of b. As the aperture becomes wider, the phase-matching condition between the pump and the generated down-conversion allows a greater range of $(\mathbf{q}, \omega)$ modes to be admitted. Those $(\mathbf{q}, \omega)$ modes that overlap less introduce more distinguishability and reduce the visibility of the quantum-interference pattern and introducing an asymmetric shape. The experimentally observed visibility for various aperture diameters, using the 1.5-mm thick BBO crystal employed in our experiments (symbols in Fig. 6), is consistent with this theory. When the pump field is pulsed, there are additional limitations on the visibility that emerge as a result of the broad spectral bandwidth of the pump field [1, 26, 2, 27]. The asymmetry of the interference pattern for increasing crystal thickness is also more visible in the pulsed than in the cw regime.

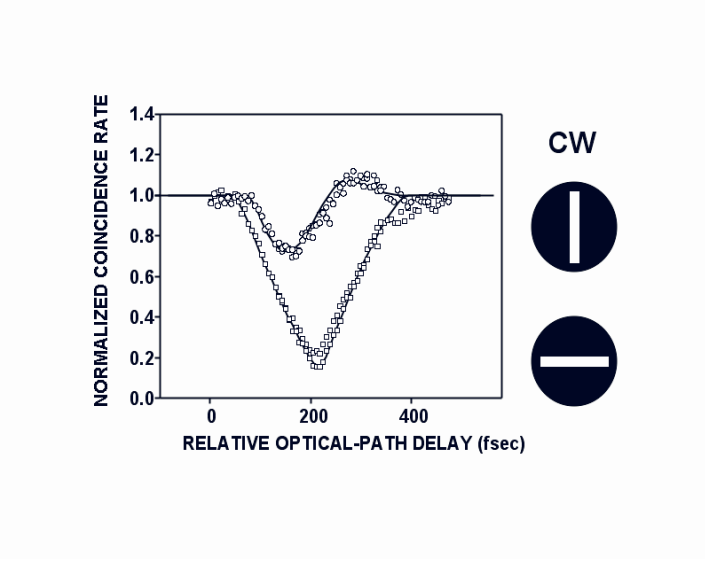

Figure 7. Normalized coincidence-count rate as a function of the relative optical-path delay for a 1×7-mm horizontal slit (circles) [23]. The data were obtained using a 351-nm cw pump and no spectral filters. Experimental results for a vertical slit are indicated by squares. Solid curves are the theoretical plots for the two orientations.

Circular apertures are used after the down-conversion crystal in the majority of quantum-interference experiments involving relative optical-path delay. However, by again departing from convention, one can also use a vertical slit

aperture to investigate the effect of and exploit *transverse* symmetry of the generated photon pairs. The solid curve of Fig. 7 shows the theoretical interference pattern expect for the vertical slit aperture. The data for the case of a horizontal slit shown by triangles is the normalized coincidence rate for a cw-pumped 1.5-mm BBO. Noting that the optical axis of the crystal falls along the vertical axis, these results verify that the dominant portion of distinguishability lies along the optical axis. The orthogonal axis (horizontal here) provides a negligible contribution to distinguishability, so that virtually full visibility is achievable, despite the wide aperture along the horizontal axis. The most dramatic effect observed is the symmetrization of the quantum-interference pattern and the recovery of the high visibility, despite the wide aperture along the horizontal axis. A practical benefit of such a slit aperture is that the count rate can be increased dramatically by limiting the range of transverse wave-vectors along the optical axis of the crystal, inducing indistinguishability and allowing a wider range along the orthogonal axis to increase the collection efficiency. A high count rate is required for many applications of entangled photon pairs. Researchers have generally suggested complex means of generating high-flux photon pairs [16], but we see that intelligent state engineering provides an elegant solution.

The optical elements in the situations above have been assumed to be placed concentrically about the longitudinal (*z*) axis. Under such circumstances, a single aperture before the beam splitter yields the same transfer function as two identical apertures placed in each arm after the beam splitter, as shown in Fig. 8. However, the quantum-interference pattern is also sensitive to a relative shift of the apertures in the transverse plane. To account for this, one must include an additional factor in Eq. (25):

$$\cos\left[\frac{\omega_p LM}{4cd_1}\frac{2\tau}{LD}\mathbf{e}_2\cdot(\mathbf{s}_A-\mathbf{s}_B)\right], \tag{29}$$

where $\mathbf{s}_i$ (with $i=A,B$) is the displacement of each aperture from the longitudinal (*z*) axis. This extra factor provides yet another degree of control on the quantum-interference pattern for a given aperture form.

As in the case of the shifted slit, $V(\tau)$ becomes negative for certain values of the relative optical-path delay (τ), and the interference pattern displays a peak rather than a triangular dip, as shown in Fig. 8, something of significant practical value. One can thus use one physical parameters to effect a change in the interference pattern associated with another parameter. In this example, observations made at the center of the interference pattern show what would be a polarization destructive interference minimum become an polarization interference maximum, when a spatial parameter (wave-vector) is altered.

The interference patterns generated in these experiments are seen to be influenced by the profiles of the apertures in the optical system, which admit wave vectors in specified directions. Including a finite bandwidth for the pump

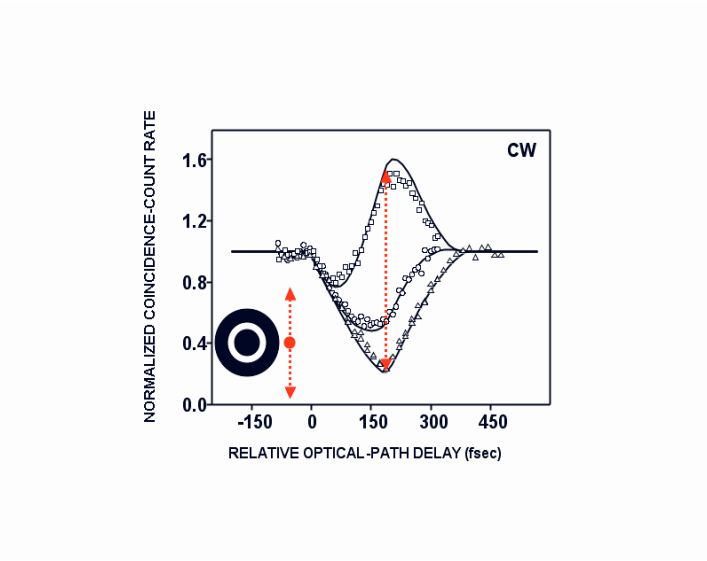

Figure 8. Inversion of the central interference feature of polarization interference through the use of spatial parameters [23]. The normalized coincidence-count rate is shown as a function of the relative optical-path delay, for an annular aperture in one of the arms of the interferometer.

field strengthens this dependence on the aperture profiles, clarifying why the asymmetry was first observed in the ultrafast regime. The multi-parameter entangled nature of the two-photon state generated by SPDC allows transverse spatial effects to play a role in polarization-based quantum-interference experiments. In contrast to the usual single-direction polarization entangled state, the wide-angle polarization-entangled state offers a richness that can be exploited in a variety of applications.

3. Quantum Metrology and Quantum Information

There are several practical applications that become available when using entangled states of light. Such states have been used with great effectiveness during the last twenty years for innovative research out definitive experiments, such as realizing non-local dispersion cancellation, entangled-photon-induced transparency, and entangled-photon spectroscopy with monochromatic light. Though each individual subsystem of an entangled system exhibits inherent uncertainties, the elements of the entangled pair may exhibit no uncertainty relative to one another. For example, while the time of arrival of an individual particle may be totally random, an entangled pair following the same path always arrives simultaneously. One can exploit this unique aspect of entan-

glement for the development of a new class of optical measurements, those of quantum optical metrology. The availability of entangled beams has made it possible to conduct such experiments without having to resort to costly instruments such as particle colliders, and synchrotrons. Non-classical correlations between photons generated in SPDC are not diminished by separations, however large, between them during propagation, even when lying outside one another's the light cone. The interferometers developed for this purpose can exploit the persistence of entanglement over distances for the purposes of quantum communications, such as in quantum cryptography.

The non-local features of two-photon entangled states have opened up new realms of high-accuracy and absolute optical metrology. The research of the last two decades has produced several new technologies: 1) Quantum key distribution, more commonly known as quantum cryptography; 2) A method for absolute measurement of photodetector quantum efficiency that does not require the use of conventional standards of optical radiation, such as blackbody radiation; 3) A technique for determining polarization-mode-dispersion with attosecond precision; 4) A method of absolute ellipsometry which requires neither source nor detector calibration, nor a reference sample. While attention here is restricted to the above four techniques, a range of other new quantum techniques has also been pursued, including quantum imaging [28, 29], optical coherence tomography [30] and quantum holography [31].

3.1 Quantum Cryptography Using Entangled Photon Pairs

The currently most advanced form of quantum information experimentation is that taking place in quantum cryptography, in particular in quantum (cryptographic) key distribution (QKD). The security of QKD is not based on complexity, but on quantum mechanics, since it is generally not possible to measure an unknown quantum system without altering it and quantum states cannot be perfectly copied [32]. The basic QKD protocols are the BB84 scheme (Bennett and Brassard [33]) and the Ekert scheme [34]. BB84 uses single photons transmitted from sender (Alice) to receiver (Bob), which are prepared at random in four partly orthogonal polarization states: 0, 45, 90 and 135 degrees. When an eavesdropper, Eve, tries to obtain information about the polarization, she introduces observable bit errors, which Alice and Bob can detect by comparing a random subset of the generated keys. By contrast, the Ekert protocol uses entangled pairs and a Bell-type inequality to transmit quantum key bits. In the Ekert scheme, both Alice and Bob receive one particle of the entangled pair. They perform measurements along at least three different directions on each side, where measurements along parallel axes are used for key generation, and those along oblique angles are used for security verification.

Several innovative experiments have been made using entangled photon pairs to implement quantum cryptography, for example [35, 36, 37]. Quantum cryptography experiments have had two principal implementations: weak coherent state realizations of QKD and those using two-photons. The latter approach made use of the nonlocal character of polarization Bell states generated by spontaneous parametric down-conversion. The strong correlation of photon pairs, entangled in both energy/time and momentum/space, eliminates the problem of excess photons faced by the coherent-state approach, where the exact number of photons actually injected is uncertain. In the entangled-photon technique, one of the pair of entangled photons is measured by the sender, confirming for the sender that the state is the appropriate one. It has thus become the favored experimental technique. The unique stability of a special two-photon polarization interferometer, initially designed to perform polarization mode dispersion measurements in optical materials, allows on to realization a method quantum key distribution that surpasses the performance of quantum cryptographic techniques using weak coherent states of light [35].

3.2 Absolute Calibration of Quantum Efficiency of Photon-counting Detectors.

One of the important, and difficult, problems in optical measurement is the absolute calibration of optical radiation intensity and the measurement of the absolute value of quantum efficiency of photodetectors, especially when they operate at the single-photon level and in the infrared spectral range. A novel technique for the measurement of the absolute value of quantum efficiency of single-photon detectors in the 0.42μm-wavelength region of the infrared spectrum with high precision has been developed [15]. This technique also does not exist in the realm of classical optics, since these required properties have their origin in vacuum fluctuations. They thus have a universal character that is everywhere present, allowing for a level of accuracy commensurate with that of a national metrology facility at every laboratory, astronomical observatory, and detector-manufacturing facility around the globe. This method also exploits the universal nature of the entangled super-correlation between entangled light quanta generated in spontaneous parametric down-conversion. As a result of the universal nature of vacuum fluctuations, this method does not require the use of an external optical standard.

Traditionally, two principal approaches for determining the absolute quantum efficiency have been used: 1) comparison with an optical signal which has well-known parameters (comprising different optical standards); and 2) measurement of an optical signal by using a preliminary calibrated photoelectric detector. The physical principle used for both the optical standard and photodetector calibration methods is the spectral distribution of the intensity of thermal

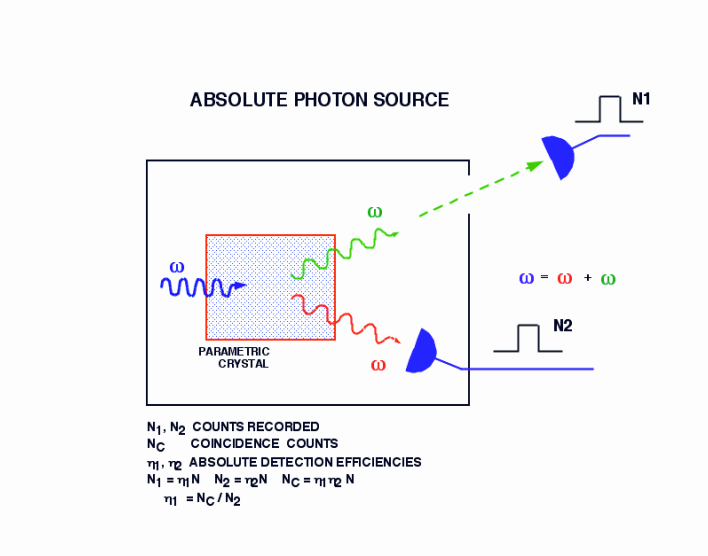

Figure 9. Principle of absolute calibration of quantum efficiency without using standards.

optical radiation, which is characterized by the Planck blackbody radiation law. Unfortunately, these techniques are useful only for the measurement of intense optical signals. They cannot be used for the measurement of optical radiation at ultra-low levels, nor for the determination of the quantum efficiency of single-photon detectors such as those required in astronomy and spectroscopy. The principle of this technique is illustrated in Fig. 9. In addition to the number of pulses registered by detector 1 (N_1) and by detector 2 (N_2), one must detect the number of coincidence counts N_C. All down-conversion photons arrive only in pairs due to their temporal correlation. The number of single photons in the two arms will also be exactly the same due to momentum correlation between the photons of each pair, so that $N_1 = N_2 = N$, which is exactly the number of pairs $N_{pairs} = N$. As a result, the absolute value of quantum efficiency is simply determined by $\eta = N_C/N_2$. In case we have a photon-number resolving detector (such as has recently been developed at NIST-Boulder), the same calibration can be performed with a single detector.

The absolute value of quantum efficiency for the photon-counting photomultiplier is derived based on the distinction between its capability of distinguishing single-photon and double-photon events. This piece of information can be evaluated by measuring the pulse-height distribution. The photodetection process is usually characterized by the value of quantum efficiency, η, that can be used as a measure of successful conversion of optical quanta into macroscopic elec-

tric signal. If the average intensity of the photon flux, *i.e.* number of photons, arriving at the surface of photodetector in the unit of time is $< N >$, then the probability of successful photodetection will be $P_1 = \eta < N >$, while that of no detection will be defined by the complimentary value $P_0 = (1-\eta) < N >$. The presence of SPDC radiation consisting of rigorously correlated photon pairs with continuous distribution in a broad spectral and angular range makes it possible to determine the spectral distribution of the measured quantities of photodetectors.

The average number of pairs $< N_{pairs} >$ per unit of time is clearly equal to the number of either signal $< N_s >$ or idler $< N_i >$ photons: $< N_s >=< N_i >=< N_{pairs} >$. From the theory of photodetection, the probability of having a double-photon event and a double-electron pulse will be $P_2 = \eta^2 < N_{pairs} >$. The probability of observing a single-photon detection event and a single-electron pulse will apparently involve the loss of one photon in the pair. Since this can happen in two different ways for every pair, the total probability of having a single-photon detection will be $P_1 = 2\eta(1-\eta) < N_{pairs} >$. One can then conclude immediately that the value of quantum efficiency can be evaluated using the following formula:

$$\eta = (1 + P_1/2P_2) - 1. \tag{30}$$

However, the gain fluctuation and thermal noise in real photodetectors usually result in a very broad pulse-height distribution corresponding to single- and double-photon detection events. This has stimulated the development of a more realistic version of this technique that would be efficient, robust, and insensitive to such imperfections in real photon-counting detectors. In order to eliminate the influence of the broad pulse-height distribution, one can use a simple comparison between the numbers of registered detection events counted: when a photodetector is exposed to a pairs of entangled photons and when exposed to a signal (or idler) photon only. The total probability of detecting an electrical pulse when pairs of entangled photons arrive at the photocathode will consist of sum of probabilities P_1 and P_2:

$$P_{pair} = P_1 + P_2 = 2\eta(1-\eta) < N_{pairs} > +\eta^2 < N_{pairs} > . \tag{31}$$

The probability of detecting a photoelectric pulse in the case of exposure to signal (or idler) photons only will be

$$P_{single} = \eta < N_s >= \eta < N_i >= \eta < N_{pairs} > \ . \tag{32}$$

The absolute value of quantum efficiency can thus be evaluated based on the results of these two measurements:

$$\eta = 2 - (P_{pair}/P_{single}) \tag{33}$$

3.3 Quantum Metrology: measurement of polarization mode dispersion with attosecond resolution.

Conventional ellipsometry techniques were developed over the years to a very high degree of performance, and are used every day in many research and industrial applications. Traditional, non-polarization-based techniques for the measurement of optical delay usually make use of monochromatic light. The introduction of an optical sample in the one arm of the interferometer causes a sudden shift of interference pattern (sometimes over tens or hundreds of wavelengths) that is proportional to the absolute value of the optical delay. This approach requires one to keep track of the total number of shifted interference fringes in order to evaluate the absolute value of the optical delay. The accuracy of this approach is limited by the stability of the interferometer, the signal-to-noise level of the detector, and the wavelength of the monochromatic radiation used. Conventional polarization interferometers used in ellipsometry measurements provide very high resolution, but have a similar problem of tracking the absolute number of 2π shifts of optical phase during the polarization-mode-dispersion measurement.

Optical engineers have come up with several ways to get around this problem, using additional complex measurement procedures. Since use of monochromatic classical polarized light does not allow one to measure the relative delay between two orthogonal waves in a single measurement, several measurements at different frequencies are used to reconstruct the polarization dispersion properties of materials. The use of highly monochromatic laser sources creates the additional problem of multiple reflections and strong irregular optical interference, especially in studying surface effects. Ellipsometry with low-coherence sources (white light) has received attention as a convenient method for the evaluation of dispersions in optical materials, particularly of communication fibers. While the technique provides the high timing resolution, along with the absolute nature of the optical delay measurement, its suffers from the problem of low visibility and instability of the interference pattern.

The unique double entanglement of the two-photon state in type-II phase-matched SPDC provides us with ultimate control of the relative position of photon pairs in space-time. The study of polarization entanglement and of the natural rectangular shape of the two-photon wave function in space-time in type-II phase-matched SPDC allows one to measure propagation time delay in optical materials with sub-femtosecond resolution. This technique intrinsically provides an absolute value of polarization optical delay that is not limited by the usual value relative to one wave cycle of light. The probe light does not disturb the physical conditions of the sample under test, and can be used continuously during the growth and assembly processes to monitor major optical parameters of the device *in situ*. By manipulating the optical delay between

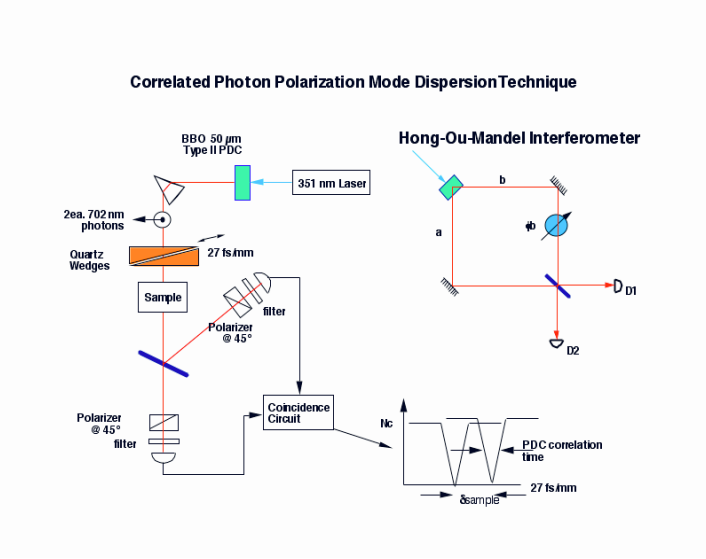

Figure 10. Schematic of a two-photon polarization interferometer.

the orthogonally polarized photons, a V-shaped correlation function feature is realized by a coincidence photon counting measurement. The general principle and a schematic experimental setup is illustrated in Fig. 10. The sharp V in the intensity correlation function can be made as narrow as 5-10 femtosecond wide. The introduction of any additional sample of optical material or photonic device with different group velocities for o-rays, (u_o,) than for e-rays, (u_e,) in the optical path before the beamsplitter will shift the V-shape distribution on a sub-femtosecond time scale. The shift is proportional to the optical delay in the sample of the length L:

$$d = (1/u_o - 1/u_e)L \approx (n_o - n_e)L/c. \tag{34}$$

In our realization, a 351nm Ar+ laser pumps the BBO crystal in a collinear and frequency-degenerate configuration. Orthogonally polarized photons generated in the BBO nonlinear crystal enter two spatially separated arms via a polarization-insensitive 50-50 beam-splitter (BS), so both ordinary and extraordinary polarized photons have equal probability of being reflected and transmitted. The two analyzers (oriented at 45 degrees) in front of each photon-counting detector D1 (D2) complete the creation of what are, in effect, two spatially separated polarization interferometers for the originally X (Y)-oriented signal and idler photons. Signal correlation is registered by coincidence events between detectors D1 and D2, as a function of a variable polarization delay (PD) in the

interferometer. Spontaneous parametric down-conversion in a BBO nonlinear crystal with L = 0.05 mm to 1 mm generates signal and idler photons with coherence lengths of tens to hundreds of femtoseconds. Such an apparatus is illustrated in Fig. 11a.

A very useful new feature realized in such an apparatus is due to the non-symmetric manipulation of the relative optical delay t between ordinary and extraordinary photons in only one of the two spatially separated interferometers. As a result, the observed coincidence probability interferogram has its triangular envelope now filled with an almost 100 percent modulation, which is associated with the period of pump radiation. The additional introduction of a sample of optical or photonic material with different o-ray and e-ray group velocities in the optical path before the beam-splitter shifts the interference pattern proportional to $\tau_{sample} = d/c$, the difference in propagation times of the two polarizations.

This allows one to measure directly the absolute value of total optical delay between two orthogonally polarized waves in the sample on a very fine, sub-femtosecond time scale. The experimental result of the measurement of intensity correlations (coincidence probability) as a function of relative polarization delay d is illustrated in Fig. 11b. The SPDC signal is delivered to the detectors without the use of any limiting spectral filters. The full width at half-maximum (FWHM) of the correlation function envelope is defined by

$$\delta = (1/u_o - 1/u_e)L_{crystal} \ . \tag{35}$$

The high visibility of the interference pattern and the extremely high stability of the polarization interferometer in such a collinear configuration allows one to identify the absolute shift of the wide envelope with an accuracy defined by the fringe size of an internal modulation.

The observed quantum interference is very high contrast, approximately 90 percent. Resolution is further enhanced by reducing the total width of the envelope. This can be done by widening the phase matching spectrum by reducing the crystal length to 50 μm. This arrangement was used to measure the optical delay of a crystal quartz sample introduced into the optical path before the beam-splitter BS. The result of this measurement (performed with the 50μm nonlinear crystal) is illustrated in Fig. 12. The 25 fs width of the envelope enables one to clearly identify the central fringe position. Based on the signal-to-noise ratio, one can expect to resolve at least 1/100 of a fringe about (10^{-17} s).

This technique for the linear polarization dispersion measurement is easy convertible to the case of circular polarization. All advantages of using quantum correlation remain. This technique can be easily modified to study optical interactions at the surfaces of materials. One can use a reflection configuration, rather than the transmission mode, and to take advantage of the strong polarization dependence of evanescent waves. This approach is a uniquely sensitive

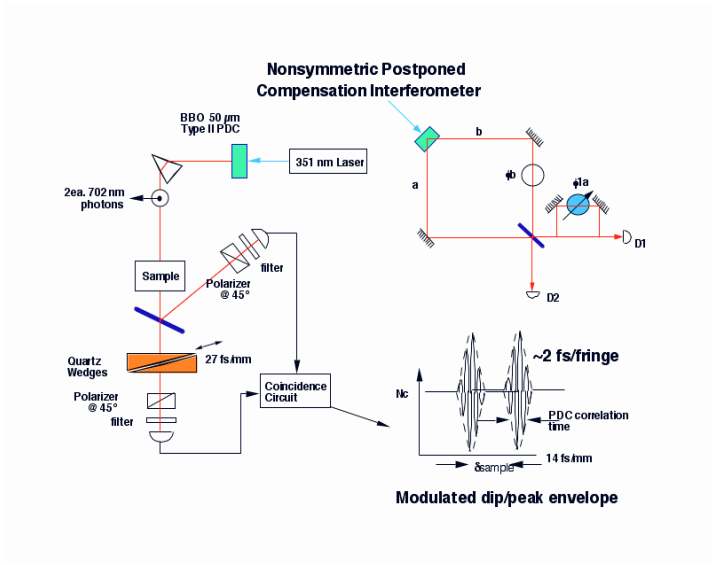

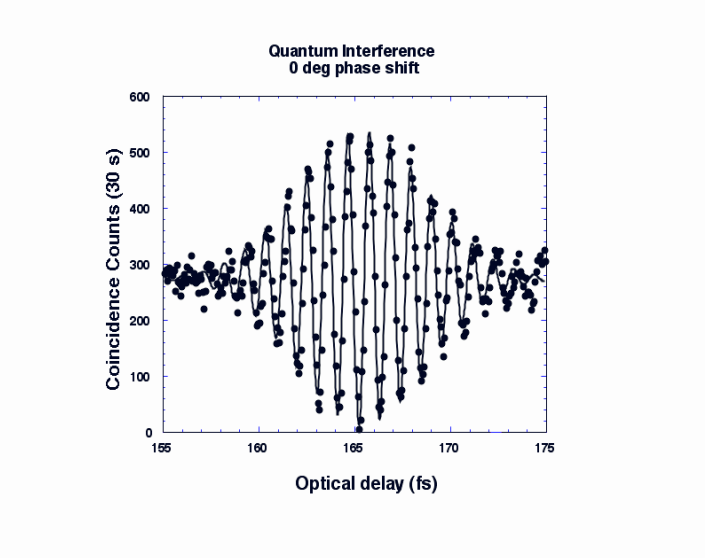

Figure 11. a) Schematic of a two-photon polarization interferometer with a postponed optical delay. This non-symmetric delay is introduced only in one arm after the beam splitter. b) Measurement of intensity correlations as a function of relative polarization delay *d*.

tool for the analysis of the orientation, structure, morphology, and optical properties of single and multiple layers of atoms either grown or deposited on a

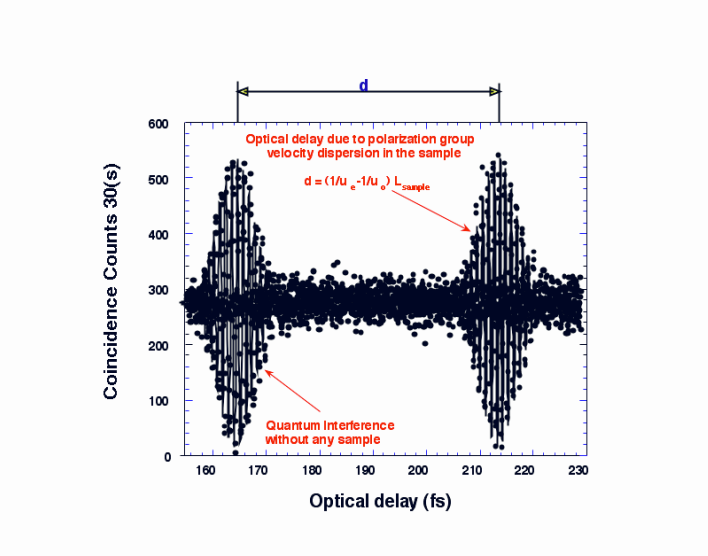

Figure 12. Measurement of the optical delay in the crystal quartz sample using a 50 μm nonlinear crystal. The horizontal scale is the time delay of the delay line located after the beamsplitter, BS.

substrate. Furthermore, if the technique can be demonstrated to be sensitive to the chemical identity of adsorbed molecules and atoms, then one can explore the application of the method to the field of chemical sensors.

3.4 Quantum Ellipsometry

In an ideal ellipsometer, the light emitted from a reliable optical source is directed into an unknown optical system and then into a reliable detector. The user keeps track of the emitted and detected radiation in order to infer information about the optical system. This device can perform ellipsometry if the source can be made to emit light of any chosen polarization. The sample is characterized by the two parameters, ψ and Δ. Parameter ψ is related to the magnitude of the ratio of the polarization (complex) reflection coefficients, $\tilde{r}_1$ and $\tilde{r}_2$, for polarization eigenstates, with $\tan\,\psi = |\tilde{r}_1/\tilde{r}_2|$, while Δ is the phase shift between them. Because of the high accuracy required in measuring these parameters, an ideal ellipsometric measurement would require absolute calibration of both the source and the detector. In practice, however, ellipsometry makes use of an array of techniques for accomodating imperfect implementations, the most common techniques being null and interferometric ellipsometry.

In a null ellipsometer, the sample is illuminated with a beam of light that can be prepared in any state of polarization. The reflected light is then analyzed. The polarization of the incident beam is adjusted to compensate for the change in the relative amplitude and phase between the polarization eigen-states introduced by the sample. The resulting reflected beam is linearly polarized. If passed through an orthogonal linear polarizer, this beam will yield a null measurement at the optical detector. This method does not require a calibrated detector, since it does not measure intensity but instead records a null result. However, it does require a reference sample to calibrate the null, for example, to find the rotational axis of reference at which an initial null is obtained, to be compared with that after inserting the sample into the apparatus. The accuracy and reliability of all measurements thus depend on our knowledge of this reference sample. Another classical technique is to employ an interferometric configuration, usually created by beam splitters. The sample is placed in one of the two interferometric paths. One can then estimate the efficiency of the detector given the source intensity, by performing measurements when the sample is removed from the interferometer. This configuration thus alleviates the problem of an unreliable detector. However, this method depends on the reliability of the source and suffers from the drawback of requiring several optical components (beam splitters, mirrors, and so on), and so depends on the parameters of these as well.

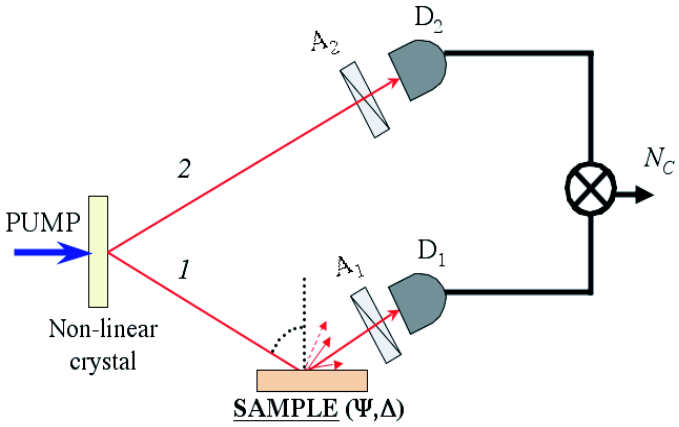

Figure 13. Entangled twin-photon ellipsometer [40].

The quantum technique again takes advantage of the characteristics of quantum states produced in type-II-phase-matched SPDC [40]. Recall that type-II phase-matching requires the signal and idler photons to have orthogonal polarizations, one extraordinary and the other ordinary. These two photons emerge from the NLC with a relative time delay, due to the birefringence of the NLC. As has been discussed above, sending the pair through an appropriate birefringent element can compensate for this time delay. This temporal compensation allows one to extract ψ and Δ. The NLC of the apparatus is adjusted to produce SPDC in a type II non-collinear configuration, as illustrated in Fig. 13.

The fields at the detectors can be found as follows. Let $\hat{a}_s(\omega)$ and $\hat{a}_i(\omega')$ be bosonic annihilation operators are the annihilation operators for the signal-frequency mode ω and idler frequency mode ω'. The twin-photon Jones vector of the field following the beam splitter is then

$$\hat{\mathbf{J}}_1 = \begin{pmatrix} j[-\hat{A}_s(\omega) + \hat{A}_i(\omega')] \\ \hat{A}_s(\omega) + \hat{A}_i(\omega') \end{pmatrix} \tag{36}$$

where $\hat{A}_s(\omega) \begin{pmatrix} 1 \\ 0 \end{pmatrix}$ $\hat{A}_i(\omega') \begin{pmatrix} 0 \\ 1 \end{pmatrix}$. The vectors $\begin{pmatrix} 1 \\ 0 \end{pmatrix}$ (horizontal) and $\begin{pmatrix} 0 \\ 1 \end{pmatrix}$ (vertical) are the Jones vectors representing orthogonal polarizations. The first element in $\hat{\mathbf{J}}_1$ is the annihilation operator of the field in beam 1, while the second element is the annihilation operator of the field in beam 2.

One can define a *photon-pair* Jones matrix by

$$\mathbf{T} = \begin{pmatrix} \mathbf{T_{11}} & \mathbf{T_{12}} \\ \mathbf{T_{21}} & \mathbf{T_{22}} \end{pmatrix} \tag{37}$$

where the $\mathbf{T_{kl}}$ are the standard (single-photon) Jones matrices describing the action of a deterministic optical element, in terms of input and output beam pairings $\mathbf{k}, \mathbf{l}$. The indices refer to the spatial modes of the input and output beams. The beams 1 and 2 impinge on the two polarization analyzers A_1 and A_2 directly, in absence of the sample, so the photon-pair Jones matrix is

$$\mathbf{T_p} = \begin{pmatrix} \mathbf{P}(-\theta_1) & 0 \\ 0 & \mathbf{P}(\theta_2) \end{pmatrix} , \tag{38}$$

where

$$\mathbf{P}(-\theta_1) = \begin{pmatrix} \cos^2\theta & \cos\theta\sin\theta\cos\theta \\ \cos\theta\sin\theta & \sin^2\theta \end{pmatrix} , \tag{39}$$

and θ_1 and θ_2 are the angles of the axes of the analyzers with respect to the horizontal direction.

The twin-photon Jones vector following the analyzers is therefore

$$\hat{\mathbf{J}}_2 = \mathbf{T_p}\hat{\mathbf{J}}_\mathbf{1} = \begin{pmatrix} j\mathbf{P}(-\theta_1)[-\hat{A}_s(\omega) + \hat{A}_i(\omega')] \\ \mathbf{P}(-\theta_2)\hat{A}_s(\omega) + \hat{A}_i(\omega') \end{pmatrix} \tag{40}$$

which yields expressions for the fields at the detectors. The positive frequency components of the field at detectors D_1 and D_2, $\mathbf{E_1^+}$ and $\mathbf{E_2^+}$ respectively, are given by

$$\mathbf{E_1^+} = j\Big[-\cos\theta_1 \int d\omega \exp(-j\omega t)\hat{a}_s(\omega) + \sin\theta_1 \int d\omega' \exp(-j\omega' t)\hat{a}_i(\omega')\Big] \begin{pmatrix} \cos\theta_1 \\ \sin\theta_1 \end{pmatrix} \tag{41}$$

$$\mathbf{E_2^+} = \Big[-\cos\theta_2 \int d\omega \exp(-j\omega t)\hat{a}_s(\omega) + \sin\theta_2 \int d\omega' \exp(-j\omega' t)\hat{a}_i(\omega')\Big] \begin{pmatrix} \sin\theta_2 \\ \cos\theta_2 \end{pmatrix} , \tag{42}$$

while the negative frequency components are given by their Hermitian conjugates. Finally, with the sample present in beam one, there is an additional effect on the Jones vector before the polarization analyzer, described by the transformation $\mathbf{T_s}$, so that we have the Jones vector $\hat{\mathbf{J_3}} = \mathbf{T_p T_s \hat{J}_1}$ where

$$\mathbf{T_s} = \begin{pmatrix} \mathbf{R} & \mathbf{0} \\ \mathbf{0} & \mathbf{I} \end{pmatrix} , \tag{43}$$

and

$$\mathbf{R} = \begin{pmatrix} \tilde{r}_1 & 0 \\ 0 & \tilde{r}_2 \end{pmatrix} . \tag{44}$$

In this case the field $\mathbf{E_2^+}$ is as before and $\mathbf{E_1^+}$ becomes

$$\mathbf{E_1^+} = j\Big[-\tilde{r}_1\cos\theta_1 \int d\omega \exp(-j\omega t)\hat{a}_s(\omega) + \tilde{r}_2\sin\theta_1 \int d\omega' \exp(-j\omega' t)\hat{a}_i(\omega')\Big] \begin{pmatrix} \cos\theta_1 \\ \sin\theta_1 \end{pmatrix} . \tag{45}$$

The coincidence rate $N_c \propto \sin^2(\theta_1 - \theta_2)$ is therefore

$$R = C[\tan\psi \cos^2\theta_1 \sin^2\theta_2 + \sin^2\theta_1 \cos^2\theta_2 + 2\sqrt{\tan\psi}\cos\Delta\cos\theta_1\cos\theta_2\sin\theta_1\sin\theta_2]. \tag{46}$$

One can then obtain C, ψ and Δ with a minimum of three measurements with different analyzer settings $\theta_2 = 0°$, $\theta_2 = 90°$ and $\theta_2 = 45°$ with θ_1 at any fixed position other than $0°$ and $90°$.

An advantage of this setup over its idealized null ellipsometric competitor is that the two arms of the ellipsometer are separate, and the light beams traverse them independently in different directions. This allows various instrumentation errors of the classical setup to be avoided. In the present case, no

optical components are placed between the source (NLC) and the sample; any desired polarization manipulation may be performed in the other arm of the entangled twin-photon ellipsometer. Entangled twin-photon ellipsometry is thus self-referencing, eliminating the necessity of constructing an interferometer altogether.

4. Conclusion

Entangled-photon states provide a natural basis for quantum measurement and quantum information processing due to their strong correlations, even when widely separated in space, in particular entangled-photon pairs created by spontaneous parametric down-conversion (SPDC). A comprehensive approach to these states has permits one to perform intelligent engineering of quantum states. The interdependence of physical parameters due to entanglement requires us to consider the full Hilbert space occupied by the entangled quantum state with its dependency on multiple variables. By exploiting this interdependence, one can modify the interference pattern associated with one parameter by manipulating other parameters.

Unique new forms of measurement can be performed using entangled quantum states. These states also allow quantum information to be encoded and this quantum information securely transmitted to a remote location, in a manner superior to other proposed quantum-mechanical methods. Practical use can thus be made of several of the correlation features present in entangled states. The unique properties of quantum systems were exploited in the practical quantum techniques that have been developed based on multiphoton interferometry.

References

[1] M., Atatüre, G. Di Giuseppe, M. D. Shaw, A. V. Sergienko, B. E. A. Saleh, and M. C. Teich, Phys. Rev. A **65,** 023808, 2002.

[2] G. Di Giuseppe, L. Haiberger, F. De Martini, and A. V. Sergienko, Phys. Rev. A **56,** R21, 1997; T. E. Keller and M. H. Rubin, Phys. Rev. A **56,** 1534, 1997; W. P. Grice, R. Erdmann, I. A. Walmsley, and D. Branning, Phys. Rev. A **57,** R2289, 1998.

[3] P. G. Kwiat, and R. Y. Chiao, Phys. Rev. A **45,** 6659 1992.

[4] H.-B. Fei, B. M. Jost, S. Popescu, B. E. A. Saleh, and M. C. Teich, Phys. Rev. Lett. **78,** 1679, 1997.

[5] B. E. A. Saleh, B. M. Jost, H.-B. Fei, and M. C. Teich, Phys. Rev. A **57,** 3972, 1998.

[6] E. Schrödinger, Naturwissenschaften **23,** 807, 1935; **23,** 823 (1935); **23,** 844, 1935 [Translation: J. D. Trimmer, Proc. Am. Phil. Soc. **124,** 323, 1980; reprinted in *Quantum Theory and Measurement*, edited by J. A. Wheeler and W. H. Zurek (Princeton University Press, Princeton, 1983)].

[7] A. Einstein, B. Podolsky and N. Rosen, Phys. Rev. **47**, 777, 1935.

[8] C.S. Wu, and I. Shaknov, The angular correlation of scattered annihilation radiation, Phys. Rev. Lett. **77**, 136, 1950 .

[9] D. Bohm, *Quantum Theory* (Prentice Hall, Englewood Cliffs, NJ, 1951) p. 614.

[10] D. Bohm, and Y. Aharonov, Phys. Rev. **108**, 1070, 1957.

[11] J. S. Bell, Physics **1**, 195, 1964.

[12] A. Aspect, J. Dalibard and G. Roger, Phys. Rev. Lett. **49**, 1804, 1982; A. Aspect, P. Grangier and G. Roger, Phys. Rev. Lett. 47, 460, 1981.

[13] N. Bloembergen, Nonlinear optics and spectroscopy, Rev. Mod. Phys. **54**, 685, 1982.

[14] D. C. Burnham, and D. L. Weinberg, Phys. Rev. Lett. **25**, 84, 1970.

[15] A. A. Malygin, A. N. Penin and A. V. Sergienko, Sov. Phys. JETP Lett. **33**, 477, 1981; A. A. Malygin, A. N. Penin and A. V. Sergienko, Sov. Phys. Dokl. **30**, 227, 1981.

[16] P. G. Kwiat, E. Waks, A.J. White, I. Appelbaum and P.H. Eberhard, Phys. Rev. A **60**, R773, 1999.

[17] B. E. A. Saleh, A. Joobeur, and M. C. Teich, Phys. Rev. A **57**, 3991, 1998.

[18] C. K. Hong, Z. Y. Ou and L. Mandel, Phys. Rev. Lett. **59**, 2044, 1987.

[19] C. K. Hong, Z. Y. Ou, and L. Mandel, Phys. Rev. Lett. **59**, 2044, 1987); P. G. Kwiat, A. M. Steinberg, and R. Y. Chiao, Phys. Rev. A **47**, R2472, 1993.

[20] J. G. Rarity and P. R. Tapster, Phys. Rev. Lett. **64,** 2495, 1990.

[21] Z. Y. Ou and L. Mandel, Phys. Rev. Lett. **61,** 50, 1988; Y. H. Shih and C. O. Alley, Phys. Rev. Lett. **61,** 2921, 1988; Y. H. Shih and A. V. Sergienko, Phys. Lett. A **191,** 201, 1994; P. G. Kwiat, K. Mattle, H. Weinfurter, A. Zeilinger, A. V. Sergienko, and Y. H. Shih, Phys. Rev. Lett. **75,** 4337, 1995.

[22] A. Joobeur, B. E. A. Saleh, and M. C. Teich, Phys. Rev. A **50,** 3349, 1994; C. H. Monken, P. H. Souto Ribeiro, and S. Pádua, Phys. Rev. A, **57,** 3123, 1998.

[23] M. Atatüre, G. Di Giuseppe, M. D. Shaw, A. V. Sergienko, B. E. A. Saleh, and M. C. Teich, Phys. Rev. A **66,** 023822, 2002 .

[24] T. B. Pittman, D. V. Strekalov, D. N. Klyshko, M. H. Rubin, A. V. Sergienko, and Y. H. Shih, Phys. Rev. A **53,** 2804, 1996.

[25] B. E. A. Saleh, A. F. Abouraddy, A. V. Sergienko, and M. C. Teich, Phys. Rev. A **62,** 043816, 2000.

[26] M. Atatüre, A. V. Sergienko, B. M. Jost, B. E. A. Saleh, and M. C. Teich, Phys. Rev. Lett. **83,** 1323, 1999.

[27] J. Peřina Jr., A. V. Sergienko, B. M. Jost, B. E. A. Saleh, and M. C. Teich, Phys. Rev. A **59,** 2359, 1999.

[28] A. F. Abouraddy, B. E. A. Saleh, A. V. Sergienko, and M. C. Teich Phys. Rev. Lett. **87**, 123602, 2001.

[29] Abouraddy, A. F., B. E. A. Saleh, A. V. Sergienko, and M. C. Teich, J. Opt. Soc. Am. B, **19**, 1174, 2002.

[30] Abouraddy, A. F., M. B. Nasr, B. E. A. Saleh, A. V. Sergienko, and M. C. Teich, Phys. Rev. A **65**, 053817, 2002.

[31] Abouraddy, A. F., B. E. A. Saleh, A. V. Sergienko, and M. C. Teich, Optics Express, **9**, pp.498, 2001.

[32] Wootters, W.K., and W.H. Zurek, Nature **299**, 802, 1982.

[33] Bennett C. H. and Brassard G., Proceedings of the International Conference on Computer Systems and Signal Processing, Bangalore, 1984, p. 175.

[34] Ekert A. K., Phys. Rev. Lett., **67**, 661, 1991.

[35] Sergienko, A.V., M. Atat¨ure, Z. Walton, G. Jaeger, B.E.A. Saleh and M.C. Teich, Phys. Rev. A **60**, R2622, 1999.

[36] Jennewein, T., C. Simon, G. Weihs, H. Weinfurter and A. Zeilinger, Phys. Rev. Lett. **84**, 4729, 2000.

[37] Tittel,W., J. Brendel, H. Zbinden and N. Gisin, Phys. Rev. Lett. **84**, 4737, 2000.

[38] Dauler E., Jaeger G., Muller A., Migdall A. and Sergienko A. V., J. Res. NIST, **104**, 1, 1999.

[39] Branning, D., Migdall, A. L., Sergienko, A. V., Phys. Rev. A, **62**, 063808, 2000.

[40] Abouraddy, A. F., K. C. Toussaint, Jr., A. V. Sergienko, B. E. A. Saleh, and M. C. Teich, J. Opt. Sci. Am. B **19** 656, 2002.